Melanie Werker and Uwe Ruschewitz*

$Cs_2Zn(CN)_4$: a first example of a non-cyano spinel of composition $A_2M(CN)_4$ with A = alkali metal and M = group 12 metal

https://doi.org/10.1515/znb-2019-0159
Received October 7, 2019; accepted October 24, 2019

Abstract: The crystal structure of monoclinic $Cs_2Zn(CN)_4$ ($C2/c$, $Z = 4$) was solved and refined from high-resolution synchrotron powder diffraction data (ESRF: Swiss-Norwegian beamline). In contrast to all other known cyanides of composition $A_2M(CN)_4$ with A = alkali metal and M = group 12 metal, which crystallize in cubic or rhombohedrally distorted spinel variants and thus with A^+ in an octahedral coordination, the Cs^+ cation in $Cs_2Zn(CN)_4$ shows an eight-fold coordination by CN^- anions of the $[Zn(CN)_4]^{2-}$ tetrahedra. Upon heating, no phase transition is observed. Instead, a reversible melting at approx. $T = 380$°C occurs.

Keywords: crystal structure; synchrotron powder diffraction; tetracyanozincate.

Dedicated to: Professor Arndt Simon on the Occasion of his 80th birthday.

1 Introduction

Despite their pronounced dumbbell-like shape compounds with CN^- or C_2^{2-} anions show a high tendency to crystallize in archetypal, sometimes distorted structure types very frequently found in oxides and fluorides, e. g. rock-salt (KCN [1], CaC_2 [2]), *anti*-fluorite (Na_2C_2 [3]), ReO_3 ($Ga(CN)_3$ [4]), *anti*-cuprite ($Zn(CN)_2$ [5]), elpasolite/cryolite ($Cs_2LiM(CN)_6$ with M = Mn, Fe, Co [6]), or spinel-type structures. Already in 1906, $K_2Zn(CN)_4$, $Tl_2Zn(CN)_4$, $K_2Cd(CN)_4$, $K_2Hg(CN)_4$, and $Tl_2Hg(CN)_4$ were recognized as compounds crystallizing with a cubic symmetry [7], and in 1922 the respective potassium compounds were unambiguously assigned to the spinel-type structure crystallizing in the cubic space group $Fd\bar{3}m$ (no. 227, $Z = 8$) [8–10]. Later on $Na_2Zn(CN)_4$, $Rb_2Zn(CN)_4$, and $Rb_2Cd(CN)_4$ were added to this class of compounds [11], which is sometimes termed the "cyano spinel" type. Some of these cyano spinels show phase transitions and a distorted rhombohedral variant ($R\bar{3}c$, $Z = 4$) was found to be a high-pressure phase of $K_2Zn(CN)_4$ [12] and a low-temperature phase of $K_2Hg(CN)_4$ [13]. For the latter it was shown that this phase transition is accompanied by a change from paraelastic (cubic) to ferroelastic (rhombohedral) behavior [13]. For $Rb_2Hg(CN)_4$ already at room temperature the slightly distorted rhombohedral phase is found, which transforms to the undistorted cubic spinel structure at approx. $T = 398$ K losing its ferroelastic properties [14]. Ternary cyanides with the general composition $A_2M(CN)_4$ with A = alkali metal and M = Zn, Cd are interesting starting materials for the respective acetylides $A_2M(C_2H)_4$ [15]. In our own studies, we came across $Cs_2Zn(CN)_4$, whose diffraction pattern did not show any similarity with a cubic or distorted rhombohedral spinel-type structure. In the following, we present the elucidation of its crystal structure and show that $Cs_2Zn(CN)_4$ crystallizes in a new and unprecedented structure type not related to the spinel structural family.

2 Experimental section

2.1 Synthesis (general)

Following the protocol described earlier [16, 17], $Cs_2Zn(CN)_4$ was synthesized from CsCN and $Zn(CN)_2$, which is commercially available, according to

$$CsF + NaCN \xrightarrow{EtOH} CsCN + NaF$$

$$2\,CsCN + Zn(CN)_2 \xrightarrow{4°C} Cs_2Zn(CN)_4$$

2.2 Synthesis of CsCN [18]

CsF (3.0381 g, 0.02 mol, 1 eq.) was dissolved in 50 mL ethanol, and under stirring 0.9802 g (0.02 mol, 1 eq.) finely

***Corresponding author: Uwe Ruschewitz,** Institut für Anorganische Chemie im Department für Chemie, Universität zu Köln, Greinstraße 6, D-50939 Köln, Germany, e-mail: uwe.ruschewitz@uni-koeln.de
Melanie Werker: Institut für Anorganische Chemie im Department für Chemie, Universität zu Köln, Greinstraße 6, D-50939 Köln, Germany

ground NaCN was added. After stirring for 3 days at room temperature the solution was filtered to remove the precipitated NaF. One hundred milliliter diethyl ether was added to the clear solution to precipitate CsCN, which was filtered off, washed with diethyl ether and dried in vacuum. The purity was checked by X-ray powder diffraction (XRPD).

2.3 Synthesis of $Cs_2Zn(CN)_4$ [17]

To a suspension of 0.1174 g (0.001 mol) $Zn(CN)_2$ in 4 mL hot deionized water CsCN was added in portions, until a clear solution was formed. This solution was concentrated by evaporating the water, until the solution started to cloud again. After 3 days in a refrigerator at 4°C the resulting crystalline material was filtered off, washed with small portions of ethanol and diethyl ether and dried in vacuum at 100°C. This product was used for all further investigations. – Elemental analysis for $C_4N_4Cs_2Zn$ (435.27 g mol^{-1}): Calcd. C 11.04, N 12.87; found C 11.31, N 12.83%. No hydrogen was detected.

2.4 Elemental analysis

Elemental analysis of carbon, hydrogen, and nitrogen was carried out with a EuroEA 3000 Analyzer (HEKAtech GmbH). Approx. 2 mg of $Cs_2Zn(CN)_4$ was filled into a tin cartridge under an argon atmosphere. Two measurements were carried out, from which a mean value was calculated.

2.5 X-ray powder diffraction (XRPD)

XRPD data was collected at room temperature on a STOE Stadi P powder diffractometer (germanium monochromator, Mo$K\alpha_1$ radiation, Mythen detector). Samples were sealed in capillaries ($\varnothing = 0.3$ mm) under inert conditions. Typical recording times are 30 min. Employing the WinXPow software suite [19], the recorded patterns were compared with theoretical patterns calculated from known structural data.

2.6 Synchrotron powder diffraction

High-resolution synchrotron powder diffraction data was recorded at the Swiss-Norwegian beamline (SNBL, BM31) [20] at the European Synchrotron (ESRF, Grenoble, France). The wavelength was calibrated with a Si standard NIST 640c to 0.49890 Å. The diffractometer is equipped with six counting channels, delivering six complete patterns collected with a small 1.18° offset in 2θ. A Si(111) analyzer crystal is mounted in front of each NaI scintillator/photomultiplier detector. Data was collected at room temperature and up to $T = 450$°C (heat blower) with steps of 0.002° (2θ) and 200 ms integration time per data point. Typical recording times were 30 min per scan. Data from all detectors were averaged and added to one pattern with local software. The WinXPow software suite [19] was used for raw data handling and visual inspection of the data. $Cs_2Zn(CN)_4$ was filled in a quartz capillary ($\varnothing = 0.7$ mm) and sealed under an argon atmosphere. The capillary was mounted on a spinning goniometer.

2.7 Structure solution

The reflections of the synchrotron powder diffraction pattern obtained at room temperature were indexed with a *C*-centered monoclinic unit cell with $a \approx 14.13$, $b \approx 9.19$, $c \approx 8.56$ Å, $\beta \approx 105.20°$ and $V \approx 1073$ Å^3 using ITO [21] within the WinXPow software system [19]. The resulting unit cell volume is in good agreement with that calculated from the sum of eight formula units CsCN [22] and four formula units $Zn(CN)_2$ [23] ($V_{calcd.} = 1028$ Å^3). The reflection conditions led to *Cc* and *C*2/*c* as possible space groups, which was confirmed by a Le-Bail fit using Jana2006 [24]. Extracted intensities of this Le-Bail fit in space group *C*2/*c* were used within Endeavour [25], in which the Cs and Zn positions were easily assigned. Introducing predefined CN units (C–N = 1.15 Å) also allowed the localization of the cyanide anions. It turned out that they occupy two crystallographically independent positions. The smooth and easily converging Rietveld refinement confirmed the correctness of the structural model.

2.8 Rietveld refinement

Rietveld refinements were carried out with Gsas [26, 27]. The unit cell obtained with Jana2006 [24] and the positional parameters of Cs, Zn, C1, N1, C2, and N2 obtained with Endeavour [25] were used as a starting model for the refinement. The C–N bond lengths were fixed using the soft constraint C–N = 1.15(2) Å. In the final refinement cycles all atoms were refined with isotropic temperature factors (U_{iso}), with the U_{iso} variables of the light atoms C and N constrained to one common value. Thus, in the final refinement cycles 36 variables were refined: *a*, *b*, *c*, β, zero shift, scale, two profile parameters (Pseudo-Voigt function), nine background parameters (Chebyshev

Table 1: Selected crystallographic data and some refinement details of the synchrotron powder diffraction measurement of $Cs_2Zn(CN)_4$.

	$Cs_2Zn(CN)_4$
Formula Weight/g · mol^{-1}	435.27
Space group, Z	$C2/c$ (no. 15), $Z=4$
a/Å	14.4641(6)
b/Å	9.1914(4)
c/Å	8.5614(3)
β/deg	109.629(2)
V/Å^3	1072.0(1)
R_p (with/without background)	0.1023/0.0921
wR_p (with/without background)	0.1359/0.2123
R_{Bragg}	0.0361
χ^2 (goodness of fit)	0.94
Data points	12 251
No. of refined parameters	36
No. of reflections	288
No. of restraints	3[a]
Background	Chebyshev function (9 terms)
Data range; step size/deg	$2.0 \le 2\theta \le 26.5$; 0.002
Instrument; detector	ESRF, BM31; 6 scintillation detectors
Radiation; wavelength λ /Å	synchrotron radiation, 0.49890
CCDC deposition number[b]	1956613

[a]N1–C1: 1.15(2) Å; N2–C2: 1.15(2) Å; $U_{iso}(N1)=U_{iso}(C1)=U_{iso}(N2)=U_{iso}(C2)$.
[b]CCDC 1956613 contains the supplementary crystallographic data for this paper. These data can be obtained free of charge from The Cambridge Crystallographic Data Centre *via* www.ccdc.cam.ac.uk/data_request/cif.

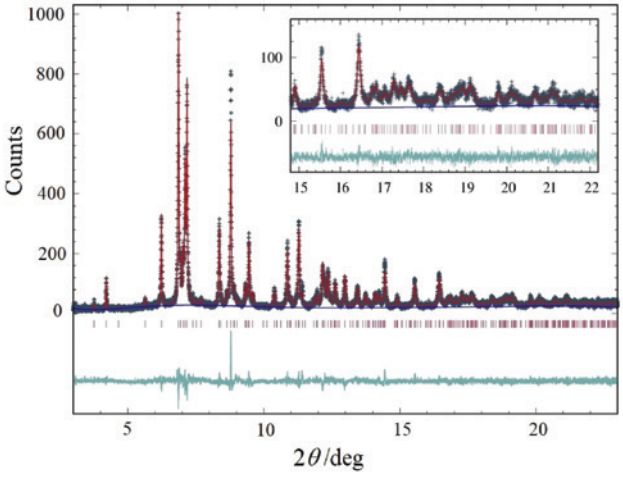

Fig. 1: Rietveld refinement of the synchrotron diffraction pattern of $Cs_2Zn(CN)_4$ (Swiss-Norwegian beamline BM31, ESRF, Grenoble, France; $\lambda = 0.49890$ Å; $T = 295(2)$ K; quartz capillary: $\varnothing = 0.7$ mm). Experimental data points (dark blue crosses), calculated profile (red solid line), background (blue solid line), and difference curve (turquoise curve below) are shown. Vertical red bars mark the positions of Bragg reflections of $Cs_2Zn(CN)_4$.

function), 16 positional parameters, and three isotropic displacement parameters. With these considerations a stable refinement leading to a smooth convergence was achieved. Selected details of the crystal structure, the measurement and the refinement are summarized in Table 1, the resulting Rietveld fit is given in Fig. 1.

2.9 Thermoanalytical investigations

DSC/TGA measurements were conducted with a TGA/DSC 1 Star^e by Mettler Toledo (Al_2O_3 crucible; Ar stream with 30 mL min^{-1}; heating rate 10 K min^{-1}). Samples of approx. 4–10 mg were weighed out and handled under inert conditions (glovebox).

2.10 IR spectroscopy

IR spectra were recorded on pure microcrystalline powders with a Bruker ALPHA FT-IR spectrometer using the ATR sample technique (diamond ATR crystal). The spectrometer was housed in a glovebox (Argon atmosphere) to provide inert conditions.

2.11 Raman spectroscopy

Raman spectra were recorded on a Renishaw InVia Quontor Raman microscope using a 457 nm Laser (laser power 1%, exposure time: 10 s), which was focused on the sample with a ×50 objective (grating: 3000 lines mm^{-1}). The spectrometer is equipped with a Centrus 05TJ CCD detector. Before and during the measurements the instrument was calibrated with an internal Si standard.

3 Results and discussion

From an aqueous solution containing $Zn(CN)_2$ and CsCN a crystalline powder of $Cs_2Zn(CN)_4$ precipitated, from which its crystal structure could be elucidated in a quite straightforward manner (see Experimental Section). Already from the resulting diffraction pattern it was obvious that $Cs_2Zn(CN)_4$ does not crystallize in a cubic or slightly distorted spinel-type variant. The resulting crystal structure is depicted in Figs. 2 and 3, atomic coordinates and selected interatomic distances and angles are listed in Table 2. As found in all cyano spinels $A_2B(CN)_4$ reported up to now, the B^{2+} cation (here: Zn^{2+}) is coordinated tetrahedrally by four

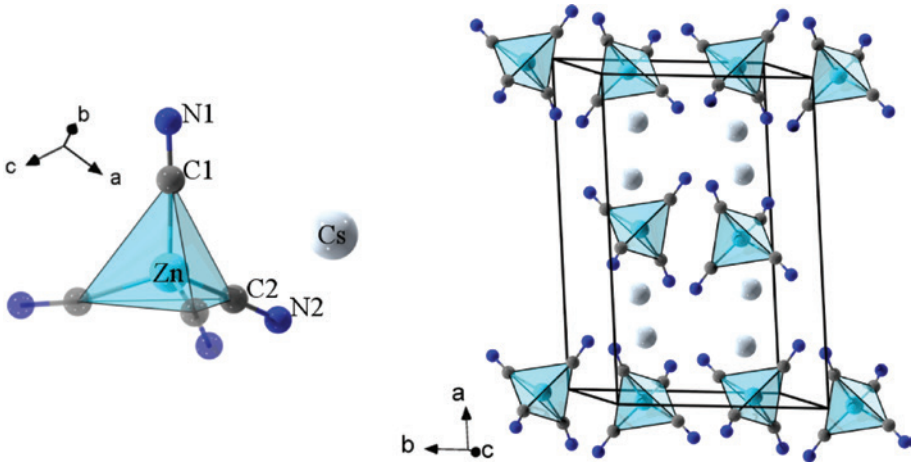

Fig. 2: Left: coordination sphere around Zn^{2+} with the atomic numbering scheme in the crystal structure of $Cs_2Zn(CN)_4$. Atoms not being part of the asymmetric unit are not numbered and drawn in a slightly transparent mode. Right: View of the unit cell of $Cs_2Zn(CN)_4$ using the same color code as in the figure on the left.

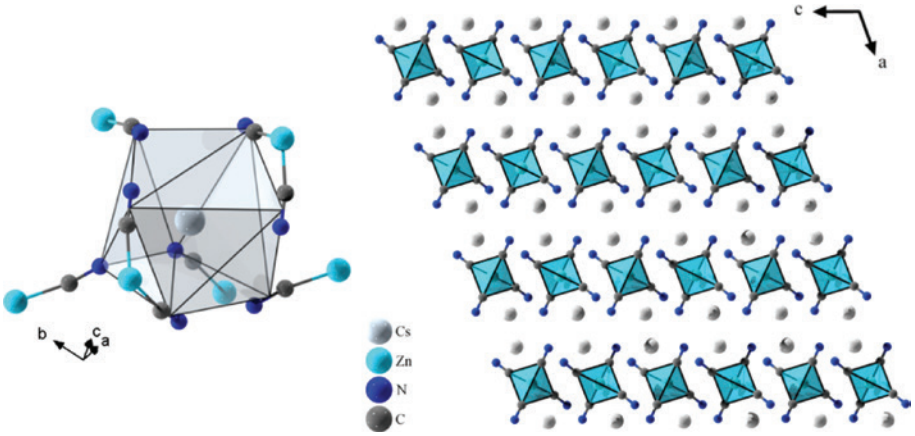

Fig. 3: Left: coordination sphere around Cs^+ in the crystal structure of $Cs_2Zn(CN)_4$. For side-on coordinating CN^- anions their center of gravity was used to draw the polyhedron around Cs^+. Right: Projection of the crystal structure of $Cs_2Zn(CN)_4$ in a view along [010]. The same color code as in Fig. 2 was used.

CN^- groups with the carbon end pointing towards Zn^{2+} [9]. The resulting $[Zn(CN)_4]^{2-}$ unit is shown in Fig. 2 (left). The C–N bond lengths were fixed to 1.15 Å in the refinement (refined to 1.155(5) Å in $K_2Zn(CN)_4$ from neutron powder diffraction data [9]), as such distances of weak scatterers like carbon and nitrogen cannot reliably be obtained from X-ray powder diffraction data. The C–Zn–C angles within the $[Zn(CN)_4]^{2-}$ tetrahedron are close to the ideal angle of 109.5° (106(1)–111(1)°, Table 2 b)) and the Zn–C–N angles deviate slightly from linearity (170(3)° and 166(3)°, Table 2b)). Slight deviations from linearity are also found in the rhombohedral variant of $K_2Zn(CN)_4$ (∠Zn–C2–N2 = 177.45° [12]), whereas in the cubic structure they are restricted to 180° for symmetry reasons. In $Cs_2Zn(CN)_4$ two crystallographically distinct CN^- anions are found. It is somewhat surprising that the Zn–C bond lengths differ by 0.13 Å: Zn–C1 = 1.84(2) Å (2×) vs. Zn–C2 = 1.97(4) Å (2×). For cubic $K_2Zn(CN)_4$ Zn–C = 2.018(4) Å (4×) [9] and for rhombohedral $K_2Zn(CN)_4$ the bond lengths Zn–C1 = 2.028 Å and Zn–C2 = 2.002 Å (3×) [12] have been reported. As the coordination spheres around $^-$C1 ≡ N1 and $^-$C2 ≡ N2 do not show distinct differences, it must be assumed that the large differences of the Zn–C1 and Zn–C2 bond lengths in $Cs_2Zn(CN)_4$ are an artefact of the refinement from X-ray powder diffraction data. The large standard deviations support this assumption. However, in $Tl_2Zn(CN)_4$ a similar spread of Zn–C bond lengths was found (1.97–2.06 Å [28]) so that these deviations are not unprecedented. The distortions within the ZnC_4 tetrahedron of $Cs_2Zn(CN)_4$ were calculated using the Continuous Shape Measures (CShM) approach by Llunell et al. [29, 30]. A low $CShM_{T-4}$ value of 0.153 points to a tetrahedron with small distortions.

Table 2: (a) Fractional atomic coordinates, isotropic displacement parameters (Å²) and (b) selected interatomic distances (Å) and angles (deg) of $Cs_2Zn(CN)_4$.

	Wyckoff position	*x*	*y*	*z*	U_{iso}
a)					
Cs	8*f*	0.3268(2)	0.1779(2)	0.2706(3)	0.049(1)
Zn	4*e*	0	0.1813(8)	1/4	0.011(2)
N1	8*f*	0.834(2)	0.995(4)	0.530(3)	0.092(5)
C1	8*f*	0.902(2)	0.939(3)	0.620(3)	0.092(5)
N2	8*f*	0.401(2)	0.864(2)	0.454(3)	0.092(5)
C2	8*f*	0.448(2)	0.808(4)	0.387(4)	0.092(5)
b)					
Zn–C1	1.84(2), 2×		C1–Zn–C2	110(1), 2×; 111(1), 2×	
Zn–C2	1.97(4), 2×		C1–Zn–C1	106(1)	
Cs–C1	3.70(3), 3.88(3), 4.03(3), 4.42(2)		C2–Zn–C2	108(1)	
Cs–N1	3.30(3), 3.65(3), 3.67(4), 3.68(3)		Zn–C1–N1	170(3), 2×	
Cs–C2	3.58(3), 3.80(4), 3.93(3), 4.21(4)		Zn–C2–N2	166(3), 2×	
Cs–N2	3.25(3), 3.29(2), 3.63(2), 3.87(2)				
C1–N1	1.15[a]				
C2–N2	1.15[a]				

[a]Fixed with soft constraints.

In Fig. 2 (right) it is shown how layers of $[Zn(CN)_4]^{2-}$ tetrahedra are separated by Cs^+ cations in $Cs_2Zn(CN)_4$. This is also obvious from the projection of the crystal structure along [010] shown in Fig. 3 (right).

In Fig. 3 (left) the coordination sphere around a Cs^+ cation is depicted. Each Cs^+ cation is surrounded by eight CN^- anions. Six of them coordinate in a side-on mode and two end-on via the nitrogen atom. The respective Cs–N bond lengths start at 3.25(3) Å and the Cs–C bond lengths at 3.58(3) Å. These CN^- groups stem from six different $[Zn(CN)_4]^{2-}$ tetrahedra so that two tetrahedra coordinate with two of their CN^- groups in a chelating fashion. This coordination of the Cs^+ cation by eight CN^- groups is different from that in the cyano spinels, where a coordination of the A^+ cation by only six CN^- anions is found. To characterize the $Cs(CN)_8$ polyhedron in more detail, the end-on coordinating CN^- groups are reduced to the coordinating nitrogen atoms and the side-on coordinating anions to their center of gravity. The resulting polyhedron is emphasized in Fig. 3 (left). Using the Continuous Shape Measures (CShM) approach [29, 30] with these eight nodes the lowest CShM value is calculated for a square antiprism with $CShM_{SAPR\text{-}8} = 2.786$. As the second best value ($CShM_{TDD\text{-}8} = 4.027$) for a trigonal dodecahedron is significantly larger, the $Cs(CN)_8$ polyhedron in $Cs_2Zn(CN)_4$ is best described by a square antiprism.

The composition of $Cs_2Zn(CN)_4$ has been further corroborated by an elemental analysis (see experimental section) and IR/Raman spectroscopic investigations (Figure S1, Supporting Information available online). The distinctive C≡N stretching vibration is found at 2148 cm^{-1} (IR) and 2146 cm^{-1} (Raman), respectively. This is in very good agreement with the results reported in the literature on comparable compounds [31] as well as our own measurements on $Rb_2Zn(CN)_4$ (2149 cm^{-1}, IR, Figure S1 (left), Supporting Information available online).

In Fig. 4 the results of a DSC/TGA measurement, heating $Cs_2Zn(CN)_4$ under inert conditions up to 1000°C, are shown. At approx. $T = 380$°C an endothermal signal is observed followed by a mass loss of 67% indicating the decomposition of the material. In Figure S2 (Supporting Information available online) the results of another DSC/TGA measurement, heating $Cs_2Zn(CN)_4$ under inert conditions up to 500°C and then cooling down to room

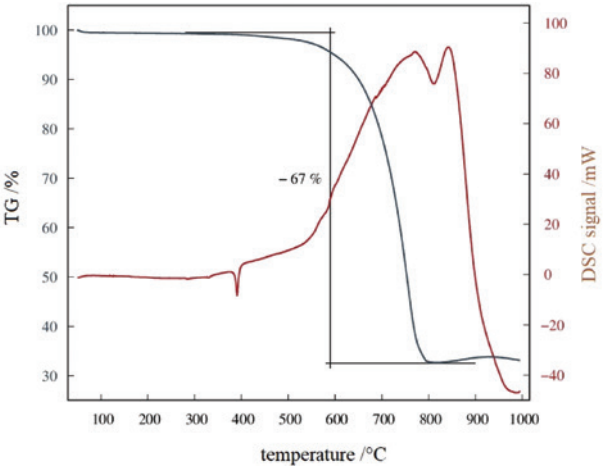

Fig. 4: DSC (red) and TGA curves (blue) of $Cs_2Zn(CN)_4$ upon heating to $T = 1000$°C under inert conditions.

temperature, are shown. The endothermal event (~380°C) is reversible with a hysteresis (approx. 300°C upon cooling). The observed minor mass loss of ~1% might be attributed to some humidity on the surface of the sample. The material obtained after heating to 500°C was analyzed by X-ray powder diffraction and compared with the starting material. The results are shown in Figure S3 (Supporting Information available online). $Cs_2Zn(CN)_4$ is obtained in a mainly unchanged form. After the heating procedure the crystallinity of the material had slightly decreased leading to a reduced signal-to-noise ratio, but no additional signals pointing to possible decomposition products are visible.

According to the cubic to rhombohedral phase transitions found in some of the cyano spinels we speculated that a similar phase transition might occur in $Cs_2Zn(CN)_4$ at approx. $T = 380$°C. To corroborate this assumption we recorded temperature-dependent synchrotron powder diffraction data at the ESRF (Swiss-Norwegian beamline). The resulting patterns are shown in Figure S4 (Supporting Information available online). At 400 and 450°C – temperatures above the endothermal event observed in the DSC measurements – the patterns indicate a completely amorphous material. Upon cooling, the resulting diffraction patterns show a different appearance and an increased crystallinity as indicated by an improved signal-to-noise ratio. This is very obvious from Figure S5 (Supporting Information available online), where the patterns obtained at 200°C upon heating and cooling are compared. However, when trying to index the resulting "new" diffraction patterns the same monoclinic unit cell was obtained. Visual inspection of the capillary indicated the formation of a solidified melt, i.e. $Cs_2Zn(CN)_4$ melts at 380°C and solidifies at approx. 300°C upon cooling. With the small focus of the synchrotron beam the resulting crystallites lead to strong preferred orientation effects explaining the "wrong", i.e. changed intensities upon cooling. The melting of the material also explains the small mass losses observed in the TGA measurements (Figure S2, Supporting Information available online), as some of the material might evaporate after melting. In Table S1 (Supporting Information available online) the results of the Rietveld (upon heating) and Le-Bail fits (upon cooling) are summarized. The calculated unit cell volumes are plotted in Fig. 5 against the temperature. The expected linear increase of the unit cell volume with increasing temperature as well as the good agreement of the volumes obtained upon heating and cooling indicate that $Cs_2Zn(CN)_4$ did not decompose. Obviously, no phase transition occurred at 380°C, but instead a reversible melting and recrystallization of the material took place. We were unable to isolate single crystals of $Cs_2Zn(CN)_4$ from the solidified melt, but we are optimistic that under improved crystallization conditions this will be feasible in the future.

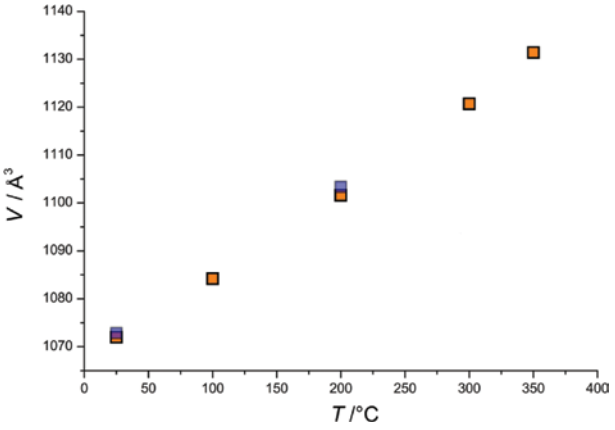

Fig. 5: Unit cell volume of $Cs_2Zn(CN)_4$ as obtained from synchrotron powder diffraction data (SNBL beamline, ESRF) upon heating (orange squares) and cooling (transparent blue squares). The calculated error bars are smaller than the symbol used for the figure.

4 Conclusion

Using high-resolution synchrotron powder diffraction data (Swiss-Norwegian beamline, ESRF, Grenoble, France) we were able to solve and refine the crystal structure of $Cs_2Zn(CN)_4$. In contrast to all other known cyanides of composition $A_2B(CN)_4$ with A = Na–Cs, Tl and B = Zn, Cd, Hg, no cubic or distorted rhombohedral spinel-type structure with A^+ in octahedral and B^{2+} in tetrahedral voids is found, but a new monoclinic structure type ($C2/c$, $Z = 4$) with B^{2+} still in tetrahedral voids, but Cs^+ in a square antiprismatic coordination of CN^- anions. Upon heating no phase transition is observed, but at approx. 380°C a melting of $Cs_2Zn(CN)_4$ occurs. We were unable to isolate single crystals from the solidified melt suitable for an X-ray single crystal structure analysis, but in the future we will try to optimize the crystallization to obtain such single crystals.

In Table 3 the ratios of the ionic radii of A^+ (coordination number: VI) and B^{2+} (coordination number: IV) according to Shannon [32] are listed for different cyanides $A_2B(CN)_4$. It is well-known that the cubic spinel-type structure can accommodate metal cations A and B with a wide range of different radii by adapting the sizes of its tetrahedral and octahedral voids. However, there seems to be a limit for this flexibility. Among all compounds listed in Table 3, $Cs_2Zn(CN)_4$ shows the highest ratio of $r(A^+)$ to $r(B^{2+})$. Obviously, this ratio is too large to be adapted by the cubic spinel-type structure and accordingly a new structure type

Table 3: Ratio of ionic radii $r(A^+)$: $r(B^{2+})$ in compounds of composition $A_2B(CN)_4$ using the ionic radii according to Shannon [32] for coordination numbers IV (B^{2+}) and VI (A^+).

	Na^+	K^+	Rb^+	Cs^+	Tl^+
Zn^{2+}	1.57	2.05	2.24	**2.45**	2.22
Cd^{2+}	1.26	1.65	1.80	1.97	1.78
Hg^{2+}	1.05	1.38	1.51	1.65	1.49

Color code: gray shading: cubic spinel-type structure; blue shading: distorted rhombohedral spinel-type structure; red shading: new monoclinic structure type (all at ambient conditions). $K_2Hg(CN)_4$ is shaded in violet, as the cubic spinel-type structure transforms to the rhombohedral variant at lower temperatures. For the unshaded entries no crystal structures have been reported up to now.

is found with a higher coordination number of Cs^+ (coordination number: VIII). For lower $r(A^+)$:$r(B^{2+})$ ratios the rhombohedrally distorted variant seems to become more likely. For example, for $K_2Hg(CN)_4$ with the lowest ratio the rhombohedral variant is found as a low-temperature phase and for $Rb_2Hg(CN)_4$ with the small value of 1.51 the rhombohedral variant is already stable at room temperature. Since it has been argued that this cubic to rhombohedral transition cannot be understood in terms of "steric interactions but must be a dynamic effect" [13], it seems to be even more interesting to clarify whether the missing members in Table 3 follow our simple "size argument". Accordingly, we expect $Na_2Cd(CN)_4$ and $Na_2Hg(CN)_4$ to crystallize in the rhombohedral variant ($R\bar{3}c$, $Z=4$).

5 Supporting information

IR and Raman spectra, DSC/TGA curve for heating and cooling in the range RT to 500°C, a comparison of X-ray powder diffraction patterns obtained as-synthesized and after heating to 500°C in the DSC/TG, temperature-dependent synchrotron powder diffraction patterns, a comparison of synchrotron powder diffraction patterns obtained at $T=200$°C and results of the Rietveld and Le-Bail fits of the temperature-dependent synchrotron powder diffraction patterns of $Cs_2Zn(CN)_4$ are given as Supplementary Material available online (DOI: 10.1515/znb-2019-0159).

Acknowledgment: We thank Dr. Hermann Emerich (ESRF) for his help with recording synchrotron powder diffraction data, Silke Kremer for elemental analysis, Laura Straub and Dr. Christoph Lenting for their help with collecting the IR/Raman spectroscopic data. The financial support of the German Science Foundation (DFG; project: RU 546/9-1) is acknowledged.

References

[1] M. Atoji, *J. Chem. Phys*. **1971**, *54*, 3514.
[2] M. Knapp, U. Ruschewitz, *Chem. Eur. J*. **2001**, *7*, 874.
[3] S. Hemmersbach, B. Zibrowius, U. Ruschewitz, *Z. Anorg. Allg. Chem*. **1999**, *625*, 1440.
[4] D. J. Williams, D. E. Partin, F. J. Lincoln, J. Kouvetakis, M. O'Keeffe, *J. Solid State Chem*. **1997**, *134*, 164.
[5] T. Kitazawa, S. I. Nishikiori, R. Kuroda, T. Iwamoto, *Dalton Trans*. **1994**, 1029.
[6] B. I. Swanson, R. R. Ryan, *Inorg. Chem*. **1973**, *12*, 283.
[7] P. Groth, *Chemische Krystallographie* – Erster Teil, 1. Auflage, **1906**.
[8] R. G. Dickinson, *J. Am. Chem. Soc*. **1922**, *44*, 774.
[9] A. Sequeira, R. Chidambaram, *Acta Crystallogr*. **1966**, *20*, 910.
[10] B. Ziegler, D. Babel, *Z. Naturforsch*. **1991**, *46b*, 47.
[11] L. D. C. Bok, J. G. Leipoldt, *Z. Anorg. Allg. Chem*. **1966**, *344*, 86.
[12] H. Ahsbahs, *Z. Kristallogr*. **1979**, *149*, 151.
[13] P. N. Gerlach, B. M. Powell, *J. Chem. Phys*. **1986**, *85*, 6004.
[14] S. Haussühl, *Acta Crystallogr*. **1978**, *A34*, 965.
[15] U. Cremer, U. Ruschewitz, *Z. Anorg. Allg. Chem*. **2004**, *630*, 337.
[16] L. C. Brousseau, D. Williams, J. Kouvetakis, M. O'Keeffe, *J. Am. Chem. Soc*. **1997**, *119*, 6292.
[17] U. Cremer, *Dissertation*, University of Cologne, Cologne **2003**.
[18] T. J. Markley, B. H. Toby, R. M. Pearlstein, D. Ramprasad, *Inorg. Chem*. **1997**, *36*, 3376.
[19] WinXPow (version 3.03; 06-Dec-2010), STOE & Cie GmbH, Darmstadt (Germany) **2010**.
[20] W. van Beek, O. V. Safonova, G. Wiker, H. Emerich, *Phase Trans*. **2011**, *84*, 726.
[21] J. W. Visser, *J. Appl. Crystallogr*. **1969**, *2*, 89.
[22] D. F. C. Morris, *Acta Crystallogr*. **1961**, *14*, 547.
[23] O. Reckeweg, A. Simon, *Z. Naturforsch*. **2002**, *57b*, 895.
[24] V. Petříček, M. Dušek, L. Palatinus, *Z. Kristallogr*. **2014**, *229*, 345.
[25] H. Putz, J. C. Schön, M. Jansen, *J. Appl. Crystallogr*. **1999**, *32*, 864.
[26] A. C. Larson, R. B. Von Dreele, Gsas, General Structure Analysis System, Report LAUR 86-748, Los Alamos National Laboratory, Los Alamos, NM (USA) **2004**.
[27] B. H. Toby, *J. Appl. Crystallogr*. **2001**, *34*, 210.
[28] L. Wiehl, P. Klüfers, B. Schweiss, H. Fuess, *Z. Kristallogr*. **1988**, *184*, 281.
[29] M. Llunell, D. Casanova, J. Cirera, P. Alemany, S. Alvarez, Shape (version 2.1), Program for the Stereochemical Analysis of Molecular Fragments by Means of Continuous Shape Measures and Associated Tools, Departament de Química Física, Departament de Química Inorgànica, and Institut de Química Teorica i Computacional, Universitat de Barcelona, Barcelona (Spain) **2013**.
[30] D. Casanova, J. Cirera, M. Llunell, P. Alemany, D. Avnir, S. Alvarez, *J. Am. Chem. Soc*. **2004**, *126*, 1755.
[31] G. W. Chantry, R. A. Plane, *J. Chem. Phys*. **1960**, *33*, 736.
[32] R. D. Shannon, *Acta Crystallogr*. **1976**, *A32*, 751.

Supplementary Material: The online version of this article offers supplementary material (https://doi.org/10.1515/znb-2019-0159).